

Instability of fluid films on a thermally conductive substrate

N. Dong and L. Kondic

Department of Mathematical Sciences, New Jersey Institute of Technology, Newark, NJ 07102 USA

(Dated: June 16, 2016)

We consider thin fluid films placed on thermally conductive substrates and exposed to time-dependent spatially uniform heat source. The evolution of the films is considered within the long-wave framework in the regime such that both fluid/substrate interaction, modeled via disjoining pressure, and Marangoni forces, are relevant. We analyze the problem by the means of linear stability analysis as well as by time-dependent nonlinear simulations. The main finding is that when self-consistent computation of the temperature field is performed, a complex interplay of different instability mechanisms results. This includes either monotonous or oscillatory dynamics of the free surface. This oscillatory behavior is absent if the film temperature is assumed to be slaved to the current value of the film thickness. The results are discussed within the context of liquid metal films, but are of relevance to dynamics of any thin film involving variable temperature of the free surface, such that the temperature and the film interface itself evolve on comparable time scales.

PACS numbers: 47.55.nb 81.16.Rf, 47.54.Jk 47.20.Dr,

I. INTRODUCTION

Instabilities of thin fluid films are relevant in a variety of different contexts, with many of these involving temperature variations that lead to modified material properties. In particular, the surface tension of many liquids is sensitive to temperature, resulting in well known Marangoni effect, that has been discussed in excellent review articles [1, 2] and books [3].

Instabilities due to Marangoni effect have been studied extensively, and we will focus here exclusively on the settings that involve deformation of the free surface. The studies are often carried out using the long-wave approach; within this framework, a significant body of work has been established in the recent years, including extensive research on linear and weakly nonlinear instability mechanisms [4–6], as well as discussion of monotone and oscillatory type of Marangoni effect governed instabilities [3, 7–9] (only a subset of relevant works is listed here). While most of the works have focused on the regime where gravitational effects are relevant, there is also an increasing body of work considering the interplay between the instabilities caused by Marangoni effect and by liquid-solid interaction that becomes important for the films on nanoscale, see, e.g., [10–13]. Understanding the influence of Marangoni effect on film stability is simplified in the settings where temperature of the film surface could be related in some simple way to its thickness; however it is not always clear that a simple functional relation can be accurately established, particularly in the setups such that the temperature field and the film thickness evolve on the comparable time scales so that the temperature of the fluid may be history dependent.

One context where thermal effects are relevant involves metal films on nanoscale thickness exposed to laser irradiation. The energy provided by laser pulses melts the films, and, while in the liquid state, these films evolve on a time scale that is often comparable to the pulse duration (tens of nanoseconds). The flow of thermal energy during this short time leads to a complex setup that involves heat flow not only in the metal film but also in the substrate, phase change (both melting and solidification), possible ablation, and chemical effects. Coupling of these effects to fluid dynamical aspects of

the problem is just beginning to be understood [12–16].

This paper focuses on fundamental mechanisms involved in the influence of thermal dependence of surface tension for films evolving on thermally conducting substrates, and therefore considers only the basic aspects of the problem, ignoring the effects of melting/solidification, ablation, or temperature dependence of other material properties. For definitiveness, we use the material parameters appropriate for liquid metals. The substrate is considered to be thermally conductive, but otherwise uniform. Since the motivation comes from nanoscale films, we do not include gravity, but we do consider substrate/film interaction via disjoining pressure model that allows for natural definition of a contact angle. It should be also noted that inclusion of fluid/solid interaction is necessary if one wants to consider film instability on nanoscale (without its inclusion, an isothermal film never breaks down, contrary to experimental findings). While, as mentioned above, a significant body of work considering the influence of Marangoni forces on thin film stability has been established, we are not aware of any work considering the interplay of Marangoni effect and fluid/solid interaction by fully self-consistent computation of the thin film evolution, and the temperature field, in fully nonlinear regime.

The rest of this papers is organized as follows. We formulate the model in Sec. II. Section III discusses the influence of Marangoni effect for a film of fixed (time-independent) thickness in Sec. III A, and then in Sec. III B for an evolving film. In Sec. III C we remove the constraint of small domain size and consider large domains that allow for mode interaction in both two and three spatial dimensions (2D and 3D). Section IV is devoted to the conclusions. The parameters used as well as derivation of the models used are given in the Appendix.

II. MODEL FORMULATION

We start by discussing in Sec. II A in rather general terms inclusion of Marangoni effect in the long-wave model. Then, in Sec. II B we focus on discussing temperature computation,

and the coupling between the evolutions of temperature, and of film thickness itself. We will see that proper accounting for film evolution when computing the temperature may be crucial for understanding the influence of Marangoni effect on film stability.

A. Thin film with Marangoni effect

We will analyze the influence of Marangoni effect within the long-wave framework that allows to obtain an insight into the most important aspects of the problems and carry out simulations at modest computational cost. The price to pay is approximate nature of the results, in particular in the context of liquid metal films that are characterized by large contact angles and fast evolution that suggests that inertial effects (not included in the standard version of the long-wave framework considered here) may be relevant. However, despite the fact that all the assumptions involved in deriving long-wave approach are not strictly satisfied, one can obtain reasonably accurate results when using the long-wave approach to explain physical experiments - see, e.g., [17–20], or even when comparing to direct numerical solvers of Navier-Stokes equations [21].

Within the long-wave framework, one reduces the complicated problem of evolving free surface film into a single 4th order nonlinear partial differential equation of diffusion type for the film thickness, h , that expresses conservation of mass of incompressible film and reads $\partial h/\partial t + \nabla \cdot (h\mathbf{v}) = 0$, where \mathbf{v} is the fluid velocity, averaged over the film thickness. This velocity can be related to the pressure gradient. To model Marangoni effect, it is typically assumed that surface tension, γ , is a linear function of temperature: $\gamma(T) = \gamma_0 + \gamma_T T$, where $\gamma_0 = \gamma(T_0)$, and γ_T is (for most of the materials) a negative constant. In the present work, T is defined relative to some reference temperature, T_0 (we will use room temperature), and non-dimensionalized as described below. In non-dimensional form, the evolution equation is as follows

$$\frac{\partial h}{\partial t} + \nabla \cdot (h^3 \nabla^2 h) + K \nabla \cdot [h^3 f'(h) \nabla h] + D \nabla \cdot (h^2 \nabla T) = 0. \quad (1)$$

Here, $\nabla = (\partial/\partial x, \partial/\partial y)$, and (x, y) are the in-plane coordinates. The second term is due to surface tension (with pressure proportional to the film curvature that is approximated by $\nabla^2 h$), and the remaining two terms are due to solid/fluid interaction and Marangoni effect, respectively. The function $f(h)$, proportional to disjoining pressure, is assumed to be of the form

$$f(h) = (h_*/h)^n - (h_*/h)^m,$$

where we use $(n, m) = (3, 2)$ as motivated by direct comparison to the experimental results for Cu films [19]. Next, we define $t_s = 3\mu l_s/\gamma_0$ as the time scale, where l_s is a chosen length-scale (we use typical film thickness of 10 nm). The non-dimensional parameters are then specified by $K = \kappa l_s/\gamma_0$, $D = 3\gamma_T/(2\gamma_0)$, and κ is related to Hamaker's constant, A , by $A = 6\pi\kappa h_*^3 l_s^3$. The reader is referred to Appendix A for

the values of the material parameters used, to [22] for extensive discussion regarding inclusion of disjoining pressure in the long-wave framework, to [15, 17, 19] for the use of the long-wave in the context of modeling liquid metal films, and to [1–3] for the discussion of Marangoni effects in a variety of settings. The numerical solutions of Eq. (1), discussed in what follows, are obtained using the spatial discretization and temporal evolution as described in e.g. [23], with the grid size equal to h_* ; such discretization is sufficient to ensure accuracy.

B. Thin film on a thermally conductive substrate

So far, the presentation applies to any situation where temperature gradients are present. Let us now focus on the setup of interest here, and that is a film exposed to an external heat source (such as a laser for experiments done with metal films), and is placed on a thermally conductive substrate, such as SiO₂. To start, consider a spatially uniform film, exposed to an energy source, and in formulating the model describing the temperature of the film, ignore convective effects, and furthermore consider only the heat flow in the z direction, normal to the plane of the film. Then, the temperature of the film (and of the substrate) can be modeled by diffusion equations (with a source term) for the film and for the substrate, coupled by appropriate boundary conditions

$$\frac{\partial T_i}{\partial t} = K_i \frac{\partial^2 T_i}{\partial z^2} + Q_i, \quad (i = 1, 2), \quad (2)$$

where $i = 1, 2$ stands for the film and for the substrate phase, respectively. The parameters entering the equation are listed in Appendix B, where we also define the temperature scale that is used throughout; here we only note that the source term, Q_1 , also includes absorption of heat in the film, and is of the functional form

$$Q_1 = CF(t) \exp(-\bar{\alpha}(z-h)), \quad (3)$$

where C is a constant determined by the intensity of the source (laser), and α is the (scaled) coefficient of absorption. We will assume that the substrate does not absorb heat ($Q_2 = 0$); this is appropriate for SiO₂ that is transparent to radiation. In fluid modeling that follows, we will also assume that the substrate remains solid. The boundary conditions include no heat transfer at the free surface; in the spirit of the long-wave approach this simplifies to $\partial T(z)/\partial z|_{z=h} = 0$ even for nonuniform films; at $z = 0$ we use continuity of temperatures and heat fluxes, therefore ignoring thermal resistance there, and at the bottom of the substrate, we put $T(-h_s) = 0$ (room temperature). Ignoring heat flow in the in-plane direction can be justified by relatively slow time scale of heat conduction in the substrate (due to low heat conductivity of SiO₂). Further studies of the importance of the in-plane heat transfer would be however appropriate and should be considered in future work. In the present work, we focus only on the main aspects of the connection between heat conduction and film evolution. We note that similar approach (of considering heat transfer in the out-of-plane direction only) has been used in existing studies, see, e.g., [15, 18].

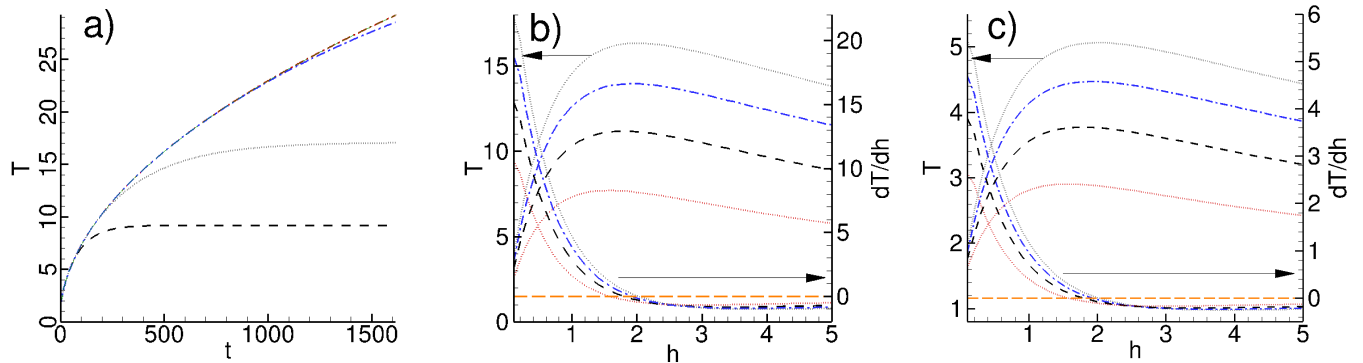


FIG. 1. (Color online) a) Temperature evolution of fixed thickness film under uniform laser pulse computed analytically assuming infinite SiO_2 thickness h_s (red dash-dotted), and numerically using $h_s = 10$ (black long dashed), $h_s = 20$ (grey dotted), $h_s = 50$ (blue dash-dotted), and $h_s = 100$ (green dashed). (Note that the numerical result with $h_s = 100$ overlaps the analytical one.) In this and all the following figures the material and laser properties are from Table 1 in Appendix A if not specified differently; in particular here laser energy density is given by E_0 . (b-c) Temperature and $\partial T/\partial h$ (with t fixed) of the free surface obtained by solving numerically Eq. (2) assuming fixed film thickness, h . Here, $t = 100$ (red dotted), $t = 200$ (black dashed), $t = 300$ (blue dash dotted), $t = 400$ (grey dotted); the arrows indicate the axis related to the set of curves. Orange long dashed line indicates $\partial T/\partial h = 0$. We use time-independent source term here, $F(T) = \text{const}$ in Eq. (3); laser energy density is E_0 (b) and $E_0/4$ (c). We show both parts (b) and (c) (that are visually similar, modulo different scales) for later reference.

III. RESULTS

We first consider in Sec. III A a film of fixed thickness, and discuss via linear stability analysis the influence that Marangoni effect has on film stability in such a setup. The temperature is here calculated either by using the analytical solution, discussed in Appendix B, or by directly solving Eqs. (2). We will see that the analytical solution gives good approximation of the temperature field as long as the substrate is sufficiently thick (in the considered setup characterized by a fixed film thickness). Then, we proceed in Sec. III B by discussing the setup where both the temperature and the film thickness evolve on comparable time scales, and show that inclusion of film thickness evolution in the formulation modifies strongly the influence of Marangoni effect on film stability: the temperature of the film is influenced considerably by the history of the film evolution. Section III C then considers the influence of Marangoni effect on film stability in large domains, both in 2D and in 3D. The parameters that are used are as given in Table 1 in Appendix A, except if specified differently.

A. Marangoni effect for a film of fixed thickness

Equations (2) are solved using standard finite difference method, with spatial derivatives discretized using central differences and Crank-Nicolson method implemented for temporal evolution; we use 160 grid points for each of the domains (film, substrate) - this value is sufficient to ensure convergence. Not surprisingly, the numerical solutions show that the temperature of the film is essentially z -independent, as also discussed in [15]. Therefore, for simplicity of notation we will from now on assume that $T = T(h, t)$. The outlined thermal

problem, for fixed (time-independent) h and in the limit of infinite substrate thickness, $h_s \rightarrow \infty$, also allows for a closed form solution for $T(h, t)$; see Appendix C for a derivation (we will refer to this solution as the analytical one). Figure 1(a) compares the analytical solution with the numerical one. We see that for large h_s there is an excellent agreement between the two, as expected. For smaller values of h_s , the numerically computed temperature saturates due to the boundary condition at $z = -h_s$. Figure 1(b) - (c) shows T and $(\partial T/\partial h)|_t$ (we omit subscript t for simplicity from now on), as a function of h . The main feature of the solution is that T is a non-monotonous function of h ; an intuitive explanation is that for thin films, only limited amount of energy gets absorbed, and the temperature remains low; for very thick films, the temperature remains low due to a large mass of the fluid that needs to be heated; as an outcome, there is a critical thickness at which T reaches a maximum value. We present results for two source energy densities that we will reference later in the text.

The next step is to couple the thermal problem with the fluid one and use the T resulting from Eq. (2) in Eq. (1). For simplicity, we will limit the consideration to two spatial dimensions so that $h = h(x, t)$ in Eq. (1). An initial insight can be reached by carrying out linear stability analysis (LSA) of a base state of flat film of thickness h_0 perturbed as follows: $h = h_0(1 + \varepsilon \exp(iqx + \sigma t))$. Assuming that T is a linear function of h (we discuss this further below), with $\partial T/\partial h = G = \text{const}$, one finds the dispersion relation

$$\sigma(q) = h_0^3 q^2 (-q^2 + P_0),$$

where

$$P_0 = Kf'(h_0) + D_1/h_0,$$

and

$$D_1 = (3\gamma_T/(2\gamma)G).$$

Then, for $P_0 > 0$, the most unstable wavelength, λ_m , and the corresponding growth rate, σ_m , are

$$\lambda_m = \frac{2\pi}{\sqrt{P_0/2}}, \quad \sigma_m = \frac{h_0^3 P_0^2}{4}. \quad (4)$$

The LSA predicts exponential decay of any perturbation for the films such that $P_0 < 0$. Considering the films of dimensionless thickness $h_0 \approx 1$, we see from Fig. 1(b) - (c) that $G > 0$ and therefore Marangoni effect is stabilizing. For thicker films, the LSA predicts increased instability; however note that for such films $|G|$ is rather small (for the present choice of parameters), and destabilizing effect of disjoining pressure is very weak, so that evolution is expected to proceed with small growth rate, suggesting that instability could occur only on very long time scales.

B. Marangoni effect for an evolving film

The analytical solution for temperature, plotted in Fig. 1 and discussed in Appendix C, as well as the numerical solutions shown in Fig. 1 assume that the film itself does not involve. However, since thermal and fluid problem are coupled, and furthermore since they evolve on comparable time scales (as it will become obvious from the following results, or based on simple dimensional arguments for the time scale governing the heat flow compared to the inverse of the growth rate for film instability), it is not clear that this assumption is appropriate, and it is also not obvious what is its influence on the results. To answer these questions, we will next consider fully coupled problem, where we solve numerically Eq. (1), while self-consistently computing the temperature by solving the system of diffusion Eqs. (2). We will first consider uniform source term, and then a Gaussian one. The initial condition is a film perturbed by a single cosine-like perturbation of the wavelength corresponding to λ_m obtained from the LSA with Marangoni effect excluded. The initial temperature (at $t = 0$) of the film and the substrate is taken to be the room temperature, so $T(t = 0) = 0$. The boundary conditions for the thin film equation (1) are of no-flux type, with the first and third derivative vanishing at the domain boundaries.

Figure 2 shows few snapshots of h , T , and $\partial T/\partial h$. Initially, (a) h is perturbed, and T is constant. The perturbation in h grows (b) due to destabilizing disjoining pressure, and leads to a perturbation in T . This perturbation stabilizes the film (the fluid flows from hot to cold), leading to essentially flat h , but T and $\partial T/\partial h$ are delayed and are not uniform (c). This nonuniform temperature induces further evolution of the film profile and ‘inverted’ perturbation (d), that is again stabilized by Marangoni flow. This process continues, leading to damped oscillatory evolution of the film.

Figure 3 shows the film thickness at the middle of the domain, $h_m = h(x_m = \lambda_m/2)$ as a function of time for few different approaches used to compute the film temperature: (i) the self-consistent time-dependent solution of Eq. (2) coupled with Eq. (1) (the same approach used to obtain the results shown in Fig. 2); (ii) the analytical solution of Eq. (2)

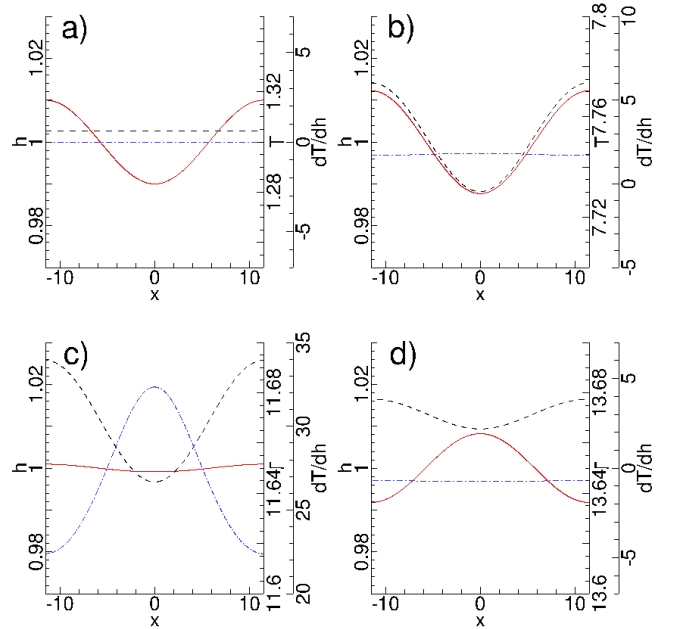


FIG. 2. (Color online) Evolution of the film thickness, h (red solid), temperature, T (black dashed), and temperature gradient, $\partial T/\partial h$ (blue dash dotted) as a result of self-consistent time-dependent computations of the film thickness and temperature. The domain size is λ_m defined by Eq. (4) without Marangoni effect ($D_1 = 0$). The times shown are: $t = 0$ (a), $t = 113$ (b), $t = 258$ (c), $t = 355$ (d).

assuming fixed film thickness, and (iii) linear temperature assuming fixed $G = 3.0$ (see Fig. 1(b)). The evolution in the absence of Marangoni effects is shown as well - here, the film destabilizes on the time scale expected from the LSA. For self-consistent temperature computations, h_m shows oscillatory behavior, in contrast to the other considered approaches for temperature computations, or when Marangoni effect is not included. Note that the numerical solution uses the substrate thickness $h_s = 100$; for such h_s , there is an excellent agreement between the numerical and analytical temperature solutions for fixed film thickness, see Fig. 1(a). Therefore, *the difference between the solutions is not due to analytical solution not being accurate, but due to the fact that it ignores evolution of the film itself.*

Our finding so far is that Marangoni effect, when included self-consistently into Eq. (1), changes dramatically the behavior of the film, leading to stabilization for the present choice of parameters. The effect is particularly strong for thin films, that are strongly unstable due to destabilizing disjoining pressure, if Marangoni effect is excluded. The obvious question is whether these results are general, in particular in the light of experimental findings that find instability, see, e.g., [13, 19]. To start answering this question, we consider the influence of two parameters: time dependence of the source term, and its total energy. The influence of the domain size and of the number of physical dimensions is discussed later in Sec. III C. Further more detailed study of the influence of other parameters will be given elsewhere [24].

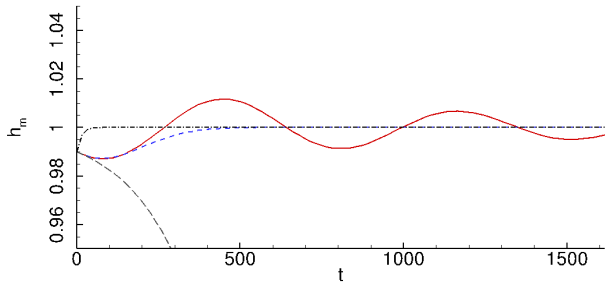


FIG. 3. The film thickness, h_m , at $x_m = \lambda_m/2$ using different approaches to compute the temperature: self-consistent time-dependent temperature computation (red solid), the analytical solution of Eq. (2) assuming fixed film thickness (blue dashed), and using fixed $G = 3.0$ obtained from Fig. 1(b) (black dash dotted). The evolution computed by ignoring Marangoni effect all together is shown as well (grey long dashed).

Figure 4 shows h_m obtained by assuming Gaussian profile (function $F(t)$) of the source of different widths (see Appendix B for more details), keeping the total energy density the same as for the uniform profile considered so far. From Fig. 4, we observe that as the energy distribution of the source becomes more narrow, the oscillatory behavior of h_m becomes stronger; however we always find that the final outcome is consistent with the one obtained for a uniform source - stable film.

Next we consider the influence of the energy density of the source term on the evolution, keeping all other parameters the same. Figures 5 and 6 show the results obtained for the same setup as the one used for Figs. 3 and 4 but with decreased energy density of the pulse. Now, the evolution is unstable: while Marangoni effect is strong enough to suppress initial instability growth (decrease of h_m), it is insufficient to stabilize the rebound: h_m increases monotonously for later times, with the final outcome (for longer times than shown in Figs. 5 and 6) of the formation of a drop centered at x_m . Other outcomes are possible: e.g, for the total energy at some intermediate level between the ones used in Figs. 4 and 6, one can find drops centered at the domain boundaries (results not shown for brevity).

To summarize, we find that Marangoni effect can have profound effect on stability of a thin film on thermally conductive substrate, and may result in oscillatory decay or growth of free surface instability. We have focused here on the influence that the source term properties have on the results; the influence of other ingredients in the model will be explored elsewhere [24]. In what follows, we discuss the influence of the domain size and its dimensionality.

C. Marangoni effect for evolving films in large domains in two and three spatial dimensions

So far we have considered influence of Marangoni effect in small computational domains and in two spatial dimensions. One may wonder whether freely evolving films, unconstrained

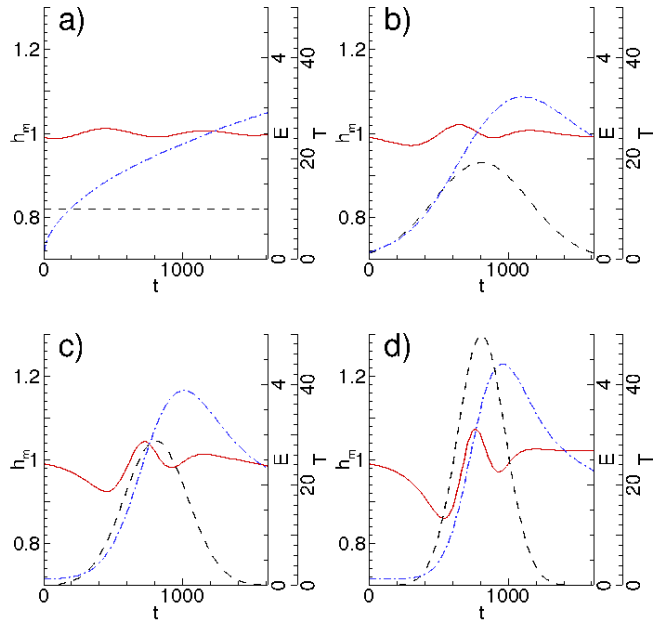


FIG. 4. The film thickness, h_m (red solid), numerically computed film temperature at x_m (blue dash dotted), and the applied energy distribution (black dashed). The total energy density applied, E_0 , during considered time window is kept constant.

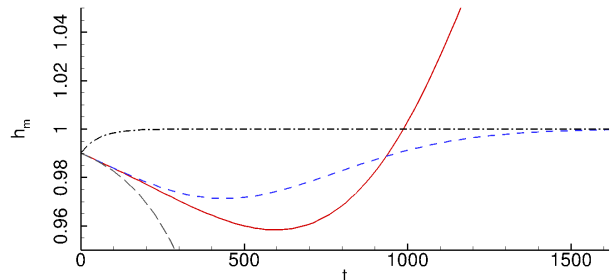


FIG. 5. The film thickness, h_m , at $x_m = \lambda_m/2$ using different approaches to compute the temperature: self-consistent time-dependent temperature computation (red solid), the analytical solution of Eq. (2) assuming fixed film thickness (blue dashed), and using fixed $G = 0.9$ obtained from Fig. 1(c) (black dash dotted). The evolution computed by ignoring Marangoni effect all together is shown as well (grey long dashed). Compare with Fig. 3 where applied energy density, and the corresponding value of G , are larger.

by domain size would evolve differently, particularly in 3D. In this section we consider evolution in large domains in both 2D and 3D and show that all the main conclusions that we have already reached remain valid; in particular, the stability properties of the films remain as we have already discussed. For brevity, we will discuss only the results obtained by fully self-consistent computation of the temperature field and resulting Marangoni effect, in addition to presenting the results of simulations that exclude Marangoni effects. Since we have not so far found strong effect of the time dependence of the source

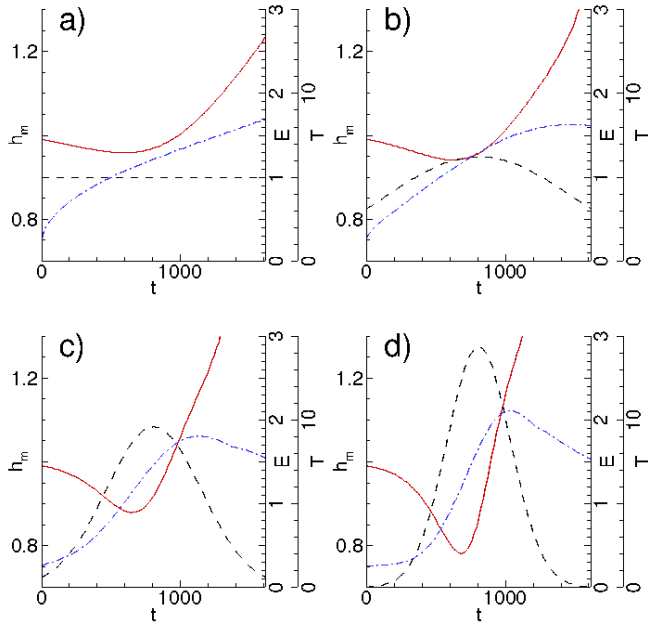


FIG. 6. The film thickness, h_m (red solid), numerically computed film temperature at x_m (blue dash dotted), and the applied energy distribution (black dashed). The total energy density applied is kept constant at $E_0/4$ (one quarter of the one used in Fig. 4). Note different scales for T and E compared to Fig. 4.

term on the evolution, we will consider only uniform source here; however, since we observed that the total applied energy density does influence the result, we will include the results for the two energy densities considered so far in this section as well.

The results that follow focus on the same time range and source properties as considered so far; this is necessary so to avoid confusion regarding total energy density provided by the heat source in Eq. (2). For this reason, some of the figures in this section (as in the preceding ones) present films that are still evolving. In the context of metal films, where films solidify after a laser pulse, any of the shown configurations may be a final one. Longer time evolution that leads to formation of drops for all considered unstable configurations, as well as the evolution for multiple laser pulses that are commonly used in experiments [13, 19, 20] will be considered in future work [24].

We consider the domain sizes that are equal to $20\lambda_m$ (with λ_m given by Eq. (4) with Marangoni effect excluded) in 2D, or to $[5\lambda_m, 5\lambda_m]$ in 3D. The 3D simulations are carried out by implementing the ADI method that has been already used in similar contexts, see e.g., [25–27] for examples, as well as [28] for a careful discussion of this method in the context of 4th order nonlinear diffusion equations. The boundary conditions are analogous to the 2D case, with the first and third derivatives vanishing in the direction normal to the domain boundary.

The initial condition consists of a film perturbed by a set of random perturbations, specified as follows. Consider $N \times N$

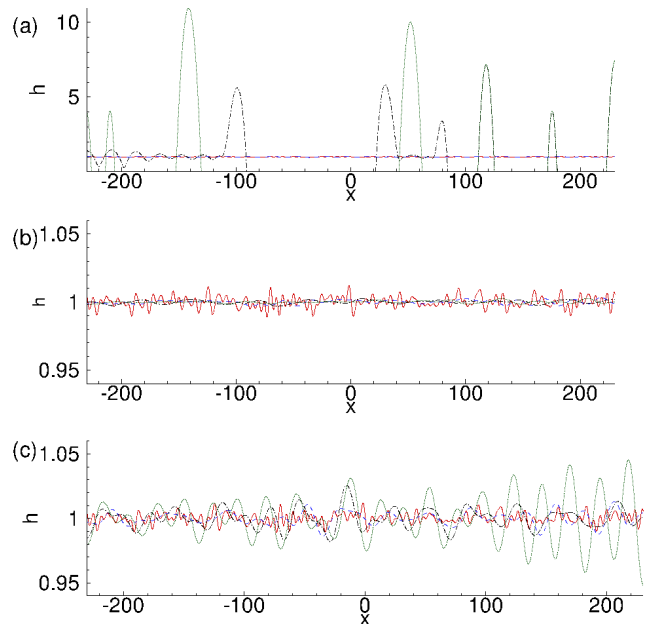


FIG. 7. The evolution of a perturbed film in a large domain (20 times the size shown in Fig. 2), the rest of the setup is the same as the one in Fig. 4 and Fig. 6, with the difference that in a) the film evolves without Marangoni effect; in b) the energy density of the source term is E_0 , the same as in Fig. 4; and in c) the energy density is $E_0/4$, the same as in Fig. 6. The initial condition is identical for all three figures and is shown by red solid lines, with the other lines showing the results at $t = 509$ (blue dashed), $t = 1074$ (black dashdot), and $t = 1583$ (green dotted).

grid in the 2D plane, with $z_{l,m}$ a random complex number of unit length. The initial condition is then specified by

$$h_{k,j} = h_0 + \varepsilon \left| \sum_{l=0}^N \left(e^{i2\pi kl/N} \sum_{m=0}^N e^{i2\pi jm/N} z_{l,m} \right) \right|. \quad (5)$$

Here, N is the number of grid points in each direction, and ε is the amplitude of perturbation. We use $\varepsilon = 0.01$ and in 2D use the 1D version of Eq. (5). Note that after this initial stochastic perturbation, the evolution is fully deterministic. See [29, 30] for further discussion of fully stochastic evolution in the context of thin film dynamics.

Figure 7 shows the evolution of randomly perturbed 2D film for three cases: without Marangoni effect (a), and with Marangoni effect included, and the total energy density applied equal to E_0 (b), and $E_0/4$ (c). We observe very different evolutions, with the instability growing quickly in (a), oscillatory instability decay in (b) and oscillatory instability growth in (c), consistently with the LSA for the no-Marangoni case, and with the results obtained in small computational domain and a single perturbation shown in the preceding figures.

During the evolution time shown in Fig. 7, the instability has only started to grow (part b)) or decay (part c)), but has already led to the formation of drops in the part a), for which Marangoni effect is excluded. This finding (implicit in the earlier figures as well) suggests that instability with and without

Marangoni effect evolves on different time scales, with faster evolution if Marangoni effect is not considered. The question of the influence of Marangoni effect on emerging length scales in the nonlinear regime of instability development is not simple to answer and its careful consideration is referred to future work [24]. Already for evolution without Marangoni effect, shown in Fig. 7, we note rather strong coarsening effect - the distance between the drops that are about to form is much larger than the most unstable wavelength, λ_m , obtained from the LSA. This coarsening is consistent with the results of simulations focusing on stochastic effects [29] and has not been, to our knowledge, carefully analyzed yet.

Next we proceed with 3D simulations. Figure 8 shows the results obtained in simulations that do not include Marangoni effect, corresponding to the ones shown in Fig. 7(a); Fig. 9 and 10 then show the results for the total energy density equal to E_0 and $E_0/4$, corresponding to Fig. 7(b) and (c), respectively. Figure 8, where final drops have already formed, shows similar coarsening effect as in 2D; the typical length scale (distance between the drops) is larger than λ_m obtained based on the LSA; similar coarsening was found when analyzing experimental results for unstable Cu films [19].

When Marangoni effect is considered, as in Figs. 9 - 10, the evolution is consistent with the 2D versions shown in Fig. 7(b) - (c). In particular, the stability properties of the films are not influenced by the geometry: the films that are unstable in 2D are unstable in 3D as well. These results show clearly strong influence of Marangoni effect on the instability evolution, suggesting that temperature dependence of surface tension may be used to control the instability development in physical experiments.

In the present work, we focus on the early stages of instability development, particularly in the case of evolution in the presence of Marangoni effect. Our future work [24] will discuss in more detail the evolution at the later stages that involve formation of drops, and the influence of Marangoni effect on the emerging length scales.

IV. CONCLUSIONS

The main conclusion of this work is that careful consideration of heat conduction is required to properly account for the influence of Marangoni forces on the film evolution: in particular, the assumption that the film temperature is slaved to its thickness leads to different results from the ones obtained by self-consistent computations. The sensitivity of the outcome as the parameters entering the problem (such as total energy density of the source term) are modified suggests that more general insight could be reached by carrying out further studies using more elaborate linear and weakly-nonlinear analyses of the evolution. We hope that our results will inspire further research in this direction.

We note that in the present work we have considered a very basic model, and have not included a number of effects: solidification and melting are not considered, modeling of heat flow is limited to one dimension; the substrate itself is considered uniform, and the other physical parameters

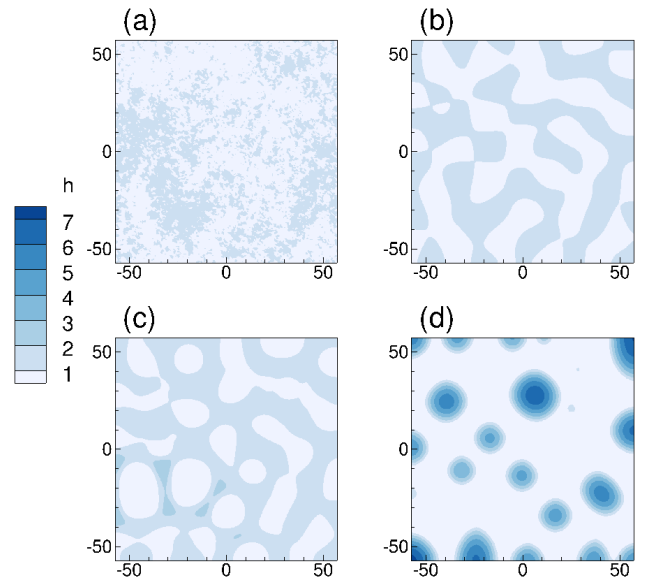


FIG. 8. The evolution of a flat film with random initial perturbation in 3D geometry. Marangoni effect is not considered. The results in this figure as well as in Figs. 9 and 10 are shown at (a) $t = 0$; (b) $t = 528$, (c) $t = 1040$, and (d) $t = 1578$.

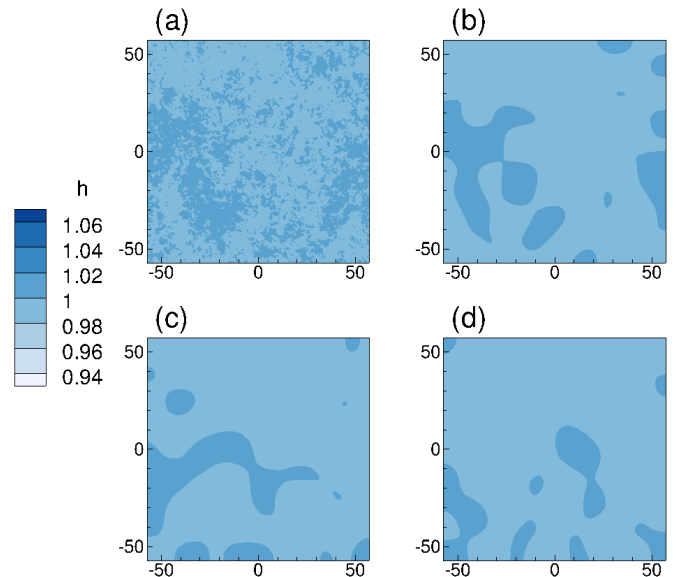


FIG. 9. The evolution of a flat film with random initial perturbation in 3D geometry. Marangoni effect is included, with the total energy density applied corresponding to E_0 .

(such as viscosity and thermal conductivity) are considered to be temperature-independent. We expect that the results presented here will serve as a basis for further improvements, in particular since they show that Marangoni effect may influence strongly both time-scales and length-scales of instability development, opening the door to its use for the purpose of controlled directed assembly on nanoscale. Our research will proceed in this direction.

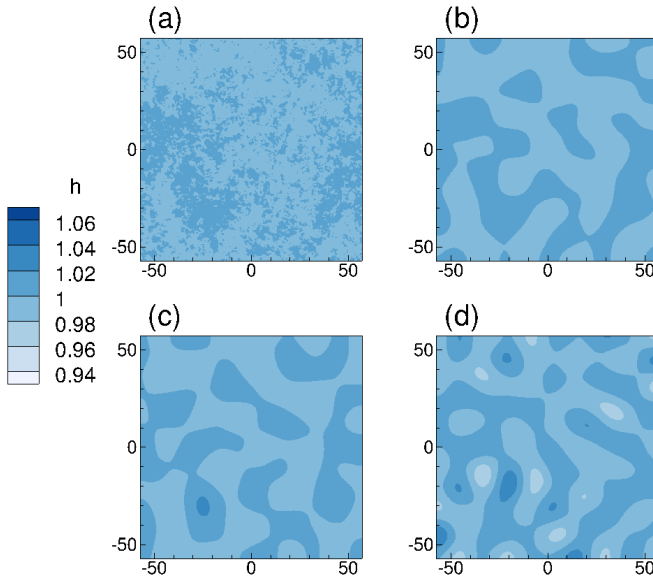


FIG. 10. The evolution of a flat film with random initial perturbation in 3D geometry. Marangoni effect is included, with the total energy density applied corresponding to $E_0/4$.

ACKNOWLEDGEMENTS

The authors thank Shahriar Afkhami, Jason Fowlkes, Kyle Mahady, Philip Rack, and Ivana Seric for many insightful discussions. This work was partially supported by the NSF Grant No. CBET-1235710.

Appendix A: Parameters

Table I provides the parameters and scales used in the main text. The film parameters (subscript ‘m’) assume Cu film, and the substrate parameters (subscript ‘s’) assume SiO₂.

Appendix B: Formulation of the heat diffusion problem

The dimensional heat diffusion equation with the time dependent source term, considered in the main text, is as follows

$$(\rho C_{eff})_m \frac{\partial T}{\partial t} = k_m \frac{\partial^2 T}{\partial z^2} + S^* F(t) \alpha_m e^{-\alpha_m(z-h)}. \quad (B1)$$

Here we take the film surface to be at $z = h$, and the film-substrate interface is at $z = 0$. In the substrate layer, the heat absorption is ignored, leading to

$$(\rho C_{eff})_s \frac{\partial T}{\partial t} = k_s \frac{\partial^2 T}{\partial z^2}. \quad (B2)$$

Parameter	Value	Unit
viscosity (μ)	4.3×10^{-3}	m ² /s
surface tension (γ)	1.303	J/m ²
length scale (l_s)	1.0×10^{-8}	m
time scale ($t_s = 3l_s\mu/\gamma$)	9.21×10^{-11}	s
film density (ρ_m)	8.0×10^3	kg/m ³
SiO ₂ density (ρ_{SiO_2})	2.2×10^3	kg/m ³
film heat capacity ($C_{eff,m}$)	4.95×10^2	J/kg/K
SiO ₂ heat capacity (C_{eff,SiO_2})	9.37×10^2	J/kg/K
film heat conductivity (k_m)	3.40×10^2	W/m/K
film absorption length (α_m^{-1})	11.09×10^{-9}	m
SiO ₂ heat conductivity (k_{SiO_2})	1.4×10^0	W/m/K
surface tension dep of T (γ_T)	-2.3×10^{-4}	J/m ²
Avogadro’s constant (A)	1.83×10^{-18}	J
reflective coefficient (r_0)	0.3655	1
film reflective length (α_r^{-1})	12.0×10^{-9}	m
laser energy density (E_0)	8.80×10^3	J/m ²
time duration of observation (t_{total})	160	ns
Gaussian pulse peak time (t_p)	80	ns
equilibrium film thickness (h_*)	1.0×10^{-10}	m
film thickness (h_0)	1.0×10^{-8}	m
SiO ₂ thickness (h_{SiO_2})	1.0×10^{-6}	m
room temperature (T_{room})	300	K

TABLE I. The parameters used in the main text.

The scales and parameters are given in Table I. For uniform pulse we have

$$S^* = [1 - R(h)] \frac{E_0}{t_p}; \quad F(t) = 1,$$

where $R(h)$ is the overall material reflectivity.

$$R(h) = r_0(1 - e^{-\alpha_r h}),$$

For Gaussian pulse,

$$S^* = [1 - R(h)] \frac{E_0 \zeta}{\sqrt{2\pi\sigma}}; \quad F(t) = \exp(-(t - t_p)^2 / \sigma^2),$$

Here, ζ is a renormalization factor used to ensure that during the considered observation time, t_{total} , the Gaussian and the uniform pulse lead to the same total applied energy.

Equation (2) from the main body of the text is obtained by using the length and time scale as defined there, and the temperature scale $T_s = t_s E_0 \alpha_m / (\rho C_{eff})_m t_p$:

$$K_1 = \frac{k_m t_s}{(\rho C_{eff})_m l_s^2},$$

$$Q_1 = \frac{t_s S^* F(t) \alpha_m e^{-\alpha_m(z-h)}}{(\rho C_{eff})_m T_s},$$

$$K_2 = \frac{k_s t_s}{(\rho C_{eff})_s l_s^2}; \quad Q_2 = 0.$$

Appendix C: Outline of the derivation of the analytical solution to the heat diffusion problem

Here, we give a brief overview of the derivation of the analytical solution of Eqs. (B1-B2), assuming that the film thickness is constant (or, equivalently, that the temperature is slaved to the current value of the film thickness), assuming also that the substrate layer is infinitely thick. This formulation was discussed in more details in [15], and also used for the purpose of estimating liquid lifetime of metal film in [16, 18, 20]. Let

$$S = \frac{S^*[1 - e^{-\alpha_m h}]}{(\rho C_{eff})_m h}; \quad K = \frac{\sqrt{(\rho C_{eff} k)_s}}{(\rho C_{eff})_m h},$$

and

$$q_s(t) = -k_m(\partial T / \partial z)_m = -k_s(\partial T / \partial z)_s.$$

Here $q_s(t)$ represents the heat flux through the film-substrate interface. Since the film layer is thin and the heat conduction high, the time scale for heat conduction in the z direction is short, $\approx 10^{-2}$ ns using the parameters as given in Table I. There, the approximation that $T \neq f(z)$ is expected to be highly accurate. Integrating Eq. (B1) from $z = h$ to $z = 0$ and taking the average, we find

$$T(t) = T_0 + \int_0^t \left(S f(\tau) - \frac{q_s(\tau)}{(\rho C_{eff})_m h} \right) d\tau. \quad (C1)$$

Solving the heat equation in the substrate of semi-infinite thickness gives

$$T_s(t, z) = T_0 + \frac{\sqrt{\alpha_s}}{k_s \sqrt{\pi}} \int_0^t q_s(\tau) (t - \tau)^{\frac{1}{2}} \exp\left(\frac{-z^2}{4\alpha_s(t - \tau)}\right) d\tau.$$

Using $T(t) = T_s(t, 0)$ we have

$$S \int_0^t f(\tau) d\tau = \int_0^t \frac{q_s(\tau) d\tau}{(\rho C_{eff})_m h} + \frac{\sqrt{\alpha_s}}{k_s \sqrt{\pi}} \int_0^t \frac{q_s(\tau)}{\sqrt{t - \tau}} d\tau.$$

Using Laplace transform, we can solve for $q_s(t)$, and substituting the result into Eq. (C1), we obtain the solution for the film temperature

$$T(t) = T_0 + S \int_0^t e^{K^2 u} \operatorname{erfc}(K\sqrt{u}) du. \quad (C2)$$

This $T(t)$ is shown in the main body of the paper as the analytical solution. Note that its derivation assumes that h remains constant in time.

-
- [1] A. Oron, S. H. Davis, and S. G. Bankoff, *Rev. Mod. Phys.* **69**, 931 (1997).
- [2] R. Craster and O. Matar, *Rev. Mod. Phys.* **81**, 1131 (2009).
- [3] P. Colinet, J. Legros, and M. Velarde, *Nonlinear dynamics of surface-tension-driven instabilities* (Wiley-VCH, Berlin, 2001).
- [4] A. Podolny, A. Oron, and A. A. Nepomnyashchy, *Phys. Fluids* **17**, 104104 (2005).
- [5] M. Morozov, A. Oron, and A. A. Nepomnyashchy, *Phys. Fluids* **27**, 082107 (2015).
- [6] A. Nepomnyashchy and I. Simanovskii, *J. Fluid Mech.* **771**, 159 (2015).
- [7] S. Shklyaev, M. Khenner, and A. A. Alabuzhev, *Phys. Rev. E* **82**, 025302 (2010).
- [8] S. Shklyaev, A. A. Alabuzhev, and M. Khenner, *Phys. Rev. E* **85**, 016328 (2012).
- [9] A. E. Samoilova and N. I. Lobov, *Phys. Fluids* **26**, 064101 (2014).
- [10] M. R. E. Warner, R. V. Craster, and O. K. Matar, *Phys. Fluids* **14**, 1642 (2002).
- [11] A. Atena and M. Khenner, *Phys. Rev. B* **80**, 075402 (2009).
- [12] M. Khenner, S. Yadavali, and R. Kalyanaraman, *Phys. Fluids* **23**, 122105 (2011).
- [13] J. Trice, D. Thomas, C. Favazza, R. Sureshkumar, and R. Kalyanaraman, *Phys. Rev. Lett.* **101**, 017802 (2008).
- [14] V. Ajaev and D. Willis, *Phys. Fluids* **15**, 3144 (2003).
- [15] J. Trice, D. Thomas, C. Favazza, R. Sureshkumar, and R. Kalyanaraman, *Phys. Rev. B* **75**, 235439 (2007).
- [16] C. A. Hartnett, K. Mahady, J. D. Fowlkes, S. Afkhami, L. Kondic, and P. D. Rack, *Langmuir* **31**, 13609 (2015).
- [17] L. Kondic, J. Diez, P. D. Rack, Y. Guan, and J. Fowlkes, *Phys. Rev. E* **79**, 026302 (2009).
- [18] J. D. Fowlkes, L. Kondic, J. Diez, and P. Rack, *Nano Letters* **11**, 2478 (2011).
- [19] A. Gonzalez, J. Diez, Y. Wu, J. Fowlkes, P. Rack, and L. Kondic, *Langmuir* **13**, 9378 (2013).
- [20] J. D. Fowlkes, N. A. Roberts, Y. Wu, J. A. Diez, A. G. González, C. Hartnett, K. Mahady, S. Afkhami, L. Kondic, and P. Rack, *Nano Letters* **14**, 774 (2014).
- [21] K. Mahady, S. Afkhami, J. Diez, and L. Kondic, *Phys. Fluids* **25**, 112103 (2013).
- [22] J. Diez and L. Kondic, *Phys. Fluids* **19**, 072107 (2007).
- [23] J. Diez and L. Kondic, *J. Comput. Phys.* **183**, 274 (2002).
- [24] N. Dong and L. Kondic, (2016), in preparation.
- [25] T.-S. Lin, L. Kondic, and A. Filippov, *Phys. Fluids* **24**, 022105 (2012).
- [26] T.-S. Lin, L. Kondic, U. Thiele, and L. J. Cummings, *J. Fluid Mech.* **729**, 214 (2013).
- [27] A. G. Gonzalez, J. D. Diez, and L. Kondic, *J. Fluid Mech.* **718**, 213 (2013).
- [28] T. Witelski and M. Bowen, *Applied Numer. Math.* **45**, 331 (2003).
- [29] S. Nestic, R. Cuerno, E. Moro, and L. Kondic, *Phys. Rev. E* **92**, 061002(R) (2015).
- [30] J. A. Diez, A. G. González, and R. Fernández, *Phys. Rev. E* **93**, 013120 (2016).